IEEE Access
Multidisciplinary | Rapid Review | Open Access Journal

Received August 10, 2019, accepted October 7, 2019, date of publication October 11, 2019, date of current version October 28, 2019.

Digital Object Identifier 10.1109/ACCESS.2019.2946899

Optimal Sampling for Dynamic Complex Networks With Graph-Bandlimited Initialization

ZHUANGKUN WEI[1], BIN LI[2], AND WEISI GUO[1,3,4], (Senior Member, IEEE)

[1]School of Engineering, University of Warwick, Coventry CV4 7AL, U.K.
[2]School of Information and Communication Engineering, Beijing University of Posts and Telecommunications, Beijing 100876, China
[3]The Alan Turing Institute, London NW1 2DB, U.K.
[4]School of Aerospace, Transport, and Manufacturing, Cranfield University, Milton Keynes MK43 0AL, U.K.

Corresponding author: Weisi Guo (weisi.guo@warwick.ac.uk)

The work of B. Li was supported in part by the Young Talent Lifting Program of China Institute of Communications under Grant QT2017001, and in part by the Natural Science Foundation of China under Grant 61971050. The work of W. Guo was supported in part by the EPSRC under Grant EP/R041725/1, in part by the Alan Turing Institute through EPSRC under Grant EP/N510129/1, and in part by the Data-Centric Engineering Program supported by the Lloyd's Register Foundation.

ABSTRACT Many engineering, social, and biological complex systems consist of dynamical elements connected via a large-scale network. Monitoring the network's dynamics is essential for a variety of maintenance and scientific purposes. Whilst we understand how to optimally sample and discretize a single continuous dynamic element or a non-dynamic graph, we do not possess a theory on how to optimally sample networked dynamical elements. Here, we study nonlinear dynamic graph signals on a fixed complex network. We define the necessary conditions for optimal sampling in the combining time- and graph-domain to fully recover the networked dynamics. We firstly interpret the networked dynamics into a linearized matrix. Then, we prove that the dynamic signals can be sampled and fully recovered if the networked dynamics is stable and their initialization and inputs (which are unknown) are bandlimited in the graph spectral domain. This new theory directly maps optimal sampling locations and rates to the graph properties and governing nonlinear dynamics. This can inform the placement of experimental probes and sensors on dynamical networks especially for the case where the employed sensors are difficult to change. Also, this guides the design of each sensor's optimal sampling rate for further digital signal processing. We motivate the reader with two examples of recovering the networked dynamics for: social population growth and networked protein biochemical interactions with both bandlimited and arbitrary initialization and inputs.

INDEX TERMS Complex network, dynamical systems, graph signal processing, sampling theory.

I. INTRODUCTION

In networked ecosystems, each element has a functional behaviour (e.g. a self-dynamic describable by a differential equation). When individual elements are coupled together via a complex network (with coupling dynamics), the whole networked system can exhibit the necessary complex behaviour [1]. There are many examples of complex networks with explicit (e.g. from phase synchronization [2] to nonlinear dynamics [3]) or latent dynamics, spanning: urban structure [4], social networks [5], economics [6], infrastructure [7], ecology [8], biology clocks [9], epidemic spreading [10], and organizational structure [11]. Whilst many such systems can be described by explicit differential equations (e.g. the mean behaviour is predictable), individual systems will differ due to usage, deterioration, and other factors. This is reflected in parameter uncertainty. As such, data monitoring of the network [12], [13] is essential for both scientific study and maintaining operational capacity. We propose to use the deterministic complex system framework to identify the optimal sampling strategy. In the context of the networked dynamical systems (see Fig. 1), we do not yet know how to optimally sample the dynamic complex networks from a joint graph- and time-domain perspective. Lack of sampling knowledge on dynamic graphs can lead to over-sampling (expensive) or under-sampling (cannot recover overall behaviour).

A. LITERATURE REVIEW

Optimal sampling for a single dynamic process is determined by the Nyquist sampling theorem. Optimal sampling on combinatorial graphs is given by the theory of spectral

The associate editor coordinating the review of this manuscript and approving it for publication was Zhong-Ke Gao.

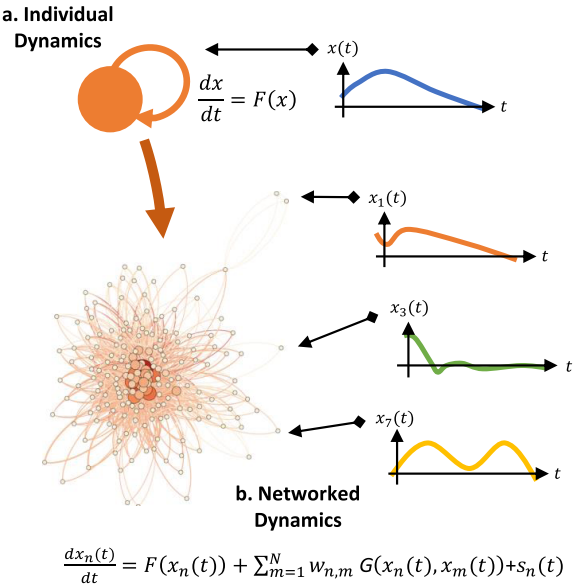

FIGURE 1. Illustration of complex network governed by dynamic equations: (a) individual dynamics, and (b) networked dynamics.

analysis [14], whereby a specific operator (e.g., the Laplacian operator, [14], [15], and the weighted adjacent matrix [16]) is employed to analyze the spectrum components. Based on these foundations, Graph Signal Processing (GSP) in recent years integrates them to understand how to sample graph signals [15]–[24]. For instance, [15] first introduced the notion of the Paley-Wiener spaces with respect to the operator on combinatorial graphs, and analyzed the graph spectrum of the signals that belong to that space. Further developments proposed the concept of the uniqueness set of nodes that can be used to sample and perfectly recover graph signals. Based on these advances, [17], [18], [20]–[23] provided several methods to find the uniqueness set. More recent work [25] considers Joint Fourier Transform (JFT) for dynamic graphs, but the sampling set changes with time, which is not useful for some real-world sensing applications (e.g. optimal sensor deployment). Whilst these studies contribute to the advancement on how to select a fixed set of sampling nodes, they cannot be used for sampling dynamic graph signals governed by explicit nonlinear dynamics - see Fig. 1, as it is difficult to design an operator that is capable of ensuring the band-limitedness of all the dynamic graph signals.

The dynamic graph signal has been studied in [26]–[30], which aimed at monitoring the dynamic graph signals (or graph process) via a subset of nodes. Specially, the state-of-the-art Kalman filter has been proposed in [30], which theoretically provides a minimum number of nodes to reconstruct the bandlimited networked dynamics from the noisy observations. However, such schemes assumed a perfect known of the bandlimited inputs, which are necessary for the inferences of the initialization and the *a posteriori* states. Whilst these inputs are generally assumed as a prior information in the context of the control system [30], [31], such assumption are a little strong for other network monitoring scenarios (e.g., the water-distribution network where the inputs are the random water-demands [32]). Moreover, there is a lack of study on how to sample a continuous networked dynamics from the combined time-graph domain. The relationship between the optimal sampling rates between graph-domain and time-domain remains unknown.

Different from the compressed sensing (e.g. a tensor) [33], [34], dynamic graphs on the one hand give explicit knowledge on its structural form, and on the other hand are governed by nonlinear dynamics that have causal relations between their time states. As such, whilst the notion of GSP with explicit dynamics shares similarities with compressed sensing, it differs in its framework and application. Notably in our work, we directly map optimal sampling locations and rates to the graph properties and governing nonlinear dynamics, which doesn't rely on data properties (e.g., the sparse structure) required by the tensor compressed sensing.

B. CONTRIBUTIONS & ORGANIZATION

In this work, we suggest a novel sampling theory from the joint time- and graph-domains for dynamic and continuous graph signals governed by explicit nonlinear dynamics. The main contributions of this paper are listed as follows.

(1) We linearize the nonlinear networked dynamics, which provides a pathway to finding the optimal graph sample set as well as the cut-off frequency from the time-domain, provided the overall network dynamics satisfy Lyapunov stability.[1] In this view, sampling the dynamic network can be viewed as time sampling on critical nodes.

(2) We provide the theory on the sampling node set for continuous graph signals. With the help of the linearized dynamics from (1), we prove that the linearized dynamic graph signals have the same graph bandwidth with the input. This indicates that we can use such bandwidth to determine the sampling node set for loss-less sampling and recovery.

(3) We prove that the graph bandwidth maps to the cut-off frequency from the time-frequency domain. This provides a guide to determine the sampling rate and discretize the continuous graph signals into digital domain for further signal processing analysis. More importantly, this relation indicates an **explicit mapping** of the optimal sampling locations and rates to the graph properties and the governing dynamics. This framework provides the dynamical system insight unavailable from previous GSP and data-driven compressed sensing research. Our fixed optimal sampling nodes also improves over current research [25] which yields dynamic sampling nodes.

(4) We evaluate our proposed sampling theory via two different application domains: (a) networked social population with linear dynamics, and (b) protein networks with nonlinear biochemical interactions. We consider both bandlimited and arbitrary inputs and the simulation results demonstrate the successful recovery of the overall networked dynamics with minimal loss. This suggests that the proposed sampling

[1] This is sensible for most stable real-world systems.

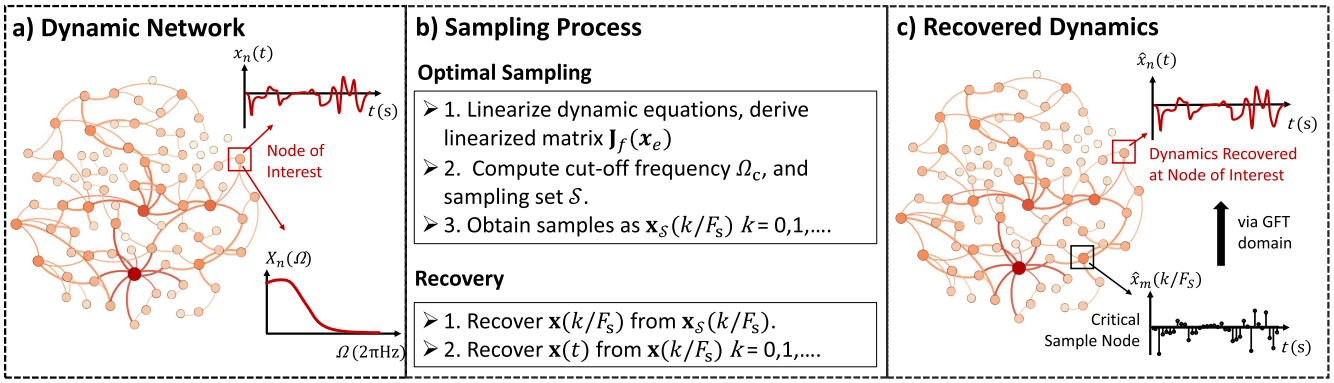

FIGURE 2. Illustration of: (a) complex network with dynamic graph signals from governing nonlinear dynamics; (b) the sampling and recovering process in terms of the combination of the time- and the graph-domain; and (c) the recovered network dynamics.

framework is beneficial to a wide range of scientific and engineering applications.

The rest of this paper is structured as follows. In Section II, we detail the networked nonlinear dynamical system model considered. In Section III, we formulate a theory on joint time- and graph-domain optimal sampling and explain the necessary conditions for recovery of the dynamics. In Section IV, we motivate the reader with two examples in networked social population dynamics and networked protein biochemical interactions. In Section V, we conclude the paper and discuss potential future areas of research.

II. SYSTEM MODEL

In this section, we provide a concept of dynamic graph signals governed by dynamic equations, and the background of the graph sampling theory.

A. SYSTEM MODEL

Signal processing on dynamic graph signals is concerned with the analysis and processing of signal-set where dynamic signal elements are connected to each other with respect to both the graph topology and the nonlinear dynamics on the node and edge (as is shown in Fig. 1). The relation is expressed through the graph $G(\mathcal{V}, \mathbf{W})$, in which $\mathcal{V} = \{1, \cdots, N\}, N \in \mathbb{N}^+$ represents a set of the subscripts of the nodes, and $\mathbf{W}$ is the adjacency matrix of the graph $G(\mathcal{V}, \mathbf{W})$. For the node v_n ($n \in \mathcal{V}$), $w_{n,m} \in \{0, 1\}$ of $\mathbf{W}$ is the directed edge from the node v_m to the node v_n. Therefore, the time-varying signal $x_n(t)$ corresponding to v_n can be described as evolving in accordance to its self-dynamic function $F(\cdot)$, an unknown input $s_n(t)$ and the mutualistic coupling function $G(x_n(t), x_m(t))$ - see Fig. 1:

$$\frac{dx_n(t)}{dt} = F(x_n(t)) + \sum_{m=1}^{N} w_{n,m} \cdot G(x_n(t), x_m(t)) + s_n(t), \quad (1)$$

$$s_n(t) = \sum_{i=1}^{+\infty} s_{n,i} \cdot \delta(t - t_i). \quad (2)$$

In Eqs. (1)-(2), the input is characterized by a group of Dirac functions $\delta(\cdot)$ placed at specific time t_i, $i \in \mathbb{N}^+$, with $s_{n,i}$ a random weight. We here denote the graph signal as $\mathbf{x}(t) = [x_1(t), \cdots, x_N(t)]^T$, and the unknown input signal as $\mathbf{s}(t) = [s_1(t), \cdots, s_N(t)]^T$ with $\mathbf{s}_i = [s_{1,i}, \cdots, s_{N,i}]^T$. Unlike the traditional graph signal that considers only a fixed data on the graph [15]–[24], we extend the concept to the time-varying signals governed by the dynamical equations.

The purpose of this paper is to study how to determine the sampling node set from graph-domain and the sampling interval from time-domain to sample and discretize the continuous networked signals and ensure the full recovery. To be specific, we should compute the sample frequency, denoted as F_s via the time-frequency perspective, as well as consider which nodes should be regarded as the sampling nodes (shown in Fig. 2), i.e., the composition of the sampling node set, denoted as $\mathcal{S} \subset \mathcal{V}$. Also, we should maintain a fixed sampling node set $\mathcal{S}$ that does **not** vary with time, as changing the sensor deployment in some real applications (e.g., the underwater surveillance) may be impractical.

B. BACKGROUND

1) APPROPRIATE SAMPLING RATE OF TIME-DOMAIN

From the perspective of sampling and discretizing a continuous signal via the time- and frequency-domain, one critical demand is to compute the cut-off frequency Ω_c, so that the discrete version is of quality for further digital signal processing (DSP). One basic method to measure the computed cut-off frequency is to resort to the Nyquist sampling interpolation.[2] By assigning the sampling frequency as $F_s \geq \Omega_c/\pi$, the time-domain signal $x(t)$ can be sampled as $x(k/F_s)$, and then recovered as:

$$\hat{x}(t) = \sum_{k \in \mathbb{Z}} x\left(\frac{k}{F_s}\right) \cdot sinc\left(F_s\left(t - \frac{k}{F_s}\right)\right), \quad (3)$$

where $sinc(t) = \sin \pi t/(\pi t)$ is the interpolation function.

[2]Note that compared to the studies in [26], [27], Nyquist sampling interpolation may not be the optimal one for signal sampling and reconstruction. But here, we are interested in the sampling rate in order to discretize the continuous signal, and we only use Nyquist theory to measure the rationality of the derived cut-off frequency.

2) GRAPH SAMPLING THEORY

Graph sampling theory samples the signal indexed on graph nodes, denoted as $\mathbf{x} = [x_1, \cdots, x_N]^T$ that has few supports on a graph Fourier transform (GFT) operator, denoted as $\mathbf{F}^{-1}$. Typically, $\mathbf{F}^{-1}$ is constructed via the eigenvectors of the Laplacian or the adjacency matrix, which are related only to the topology of the graph. Here we describe the graph sampling theory via the adjacency matrix, and the GFT operator $\mathbf{F}^{-1}$ can be given as: [16], [18],

$$\mathbf{W} = \mathbf{F} \cdot diag\{\lambda_1, \lambda_2, \cdots, \lambda_N\} \cdot \mathbf{F}^{-1}, \tag{4}$$

where $\lambda_1, \lambda_2, \cdots, \lambda_N$ are the arbitrarily ordered eigenvalues (also referred as the graph spectral values). In this setting, the graph sampling theory defines a bandlimited signal, and provides the method to sample such signals as follows:

Definition 1: [18] A graph signal $\mathbf{x}$ is called $\mathcal{R}$-bandlimited with respect to the GFT operator $\mathbf{F}^{-1}$, if all the subscripts of non-zeros in $\tilde{\mathbf{x}} = \mathbf{F}^{-1}\mathbf{x}$ compose the band-set $\mathcal{R}$.[3]

Definition 2: [18] $BL(\mathcal{R}, \mathbf{F}^{-1})$ is defined as a subspace of $\mathbb{R}^N$, composed of all $\mathcal{R}$-bandlimited graph signals with respect to $\mathbf{F}^{-1}$.

Theorem 1: [15]–[24], [35] For any $\mathbf{x} \in BL(\mathcal{R}, \mathbf{F}^{-1})$, there exists a subset $\mathcal{S} \subset \mathcal{V}$ such that

$$\mathbf{x} = \mathbf{F}_{\mathcal{VR}} \cdot (\mathbf{F}_{\mathcal{SR}}^T \cdot \mathbf{F}_{\mathcal{SR}})^{-1} \cdot \mathbf{F}_{\mathcal{SR}}^T \cdot \mathbf{x}_{\mathcal{S}}. \tag{5}$$

Such $\mathcal{S}$ satisfies

$$rank\ (\mathbf{F}_{\mathcal{SR}}) = |\mathcal{R}|, \tag{6}$$

where $\mathbf{F}_{\mathcal{SR}}$ ($\mathbf{F}_{\mathcal{VR}}$) denotes the sub-matrix of $\mathbf{F}$ with rows selected via subscripts in $\mathcal{S}$ ($\mathcal{V}$) and columns selected via subscripts in $\mathcal{R}$, and $\mathbf{x}_{\mathcal{S}}$ denotes the sampled vector of $\mathbf{x}$ by selecting subscripts in $\mathcal{S}$.

It is noteworthy that directly utilizing the graph sampling theory to identify the sampling node set $\mathcal{S}$ for dynamic networked signal $\mathbf{x}(t)$ is challenging. The operators that are related only with the graph topology (e.g., the adjacency matrix, and the Laplacian matrix) cannot maintain that the evolved signals with different time belong to the identical $BL(\mathcal{R}, \mathbf{F}^{-1})$. Saying $\mathbf{x}(t_1) \in BL(\mathcal{R}, \mathbf{F}^{-1})$, then we cannot ensure $\mathbf{x}(t_2) \in BL(\mathcal{R}, \mathbf{F}^{-1})$, for $t_1 \neq t_2$ given the dynamics. This will cause $\mathcal{R} = \{1, \cdots, N\}$, and inevitably $\mathcal{S} \equiv \mathcal{V}$, or at least a time-varying sampling node set for different time, i.e., $\mathcal{S}_{t_1} \neq \mathcal{S}_{t_2}$. In this view, it is demanding to study how to maintain the dynamic $\mathbf{x}(t)$ being $\mathcal{R}$-bandlimited with respect to some operator that combines both the graph topology and the underlying dynamics, and here come our work.

[3]It is true that the cardinality of $\mathcal{R}$ can be $|\mathcal{R}| = r < N$, indicating a similar concept of r-sparse transformation of signal $\mathbf{x}$. Different from the concept of r-sparse vector in compressed sensing where the positions of the non-zero elements are unknown, in the case of graph sampling theory, we know the positions (subscripts) of these non-zero elements. Hence, the size of the sampling node set $|\mathcal{S}|$ can be smaller as opposed to that used by compressed sensing [18].

III. SAMPLING FOR DYNAMIC GRAPH SIGNAL

In this section, we elaborate our sampling theory on dynamic graph signals. We aim to find the sampling node set $\mathcal{S} \subset \mathcal{V}$ from the graph domain, and the cut-off frequency Ω_c from the time-frequency domains. So, the discrete samples on nodes in $\mathcal{S}$ can be derived as

$$\mathbf{X}_{\mathcal{S}} = \begin{bmatrix} x_{n_1}(0/F_s) & \cdots & x_{n_1}(K/F_s) \\ \vdots & \ddots & \vdots \\ x_{n_{|\mathcal{S}|}}(0/F_s) & \cdots & x_{n_{|\mathcal{S}|}}(K/F_s), \end{bmatrix} \tag{7}$$

where $F_s \geq \Omega_c/\pi$ is the sampling frequency, $\{n_1, \cdots, n_{|\mathcal{S}|}\} = \mathcal{S}$, and K/F_s represents the total time that is of interest. The recovered signal $\hat{\mathbf{x}}(t)$ will be computed as:

$$\hat{\mathbf{x}}(t) = \mathbf{\Phi} \cdot \mathbf{X}_{\mathcal{S}} \cdot \mathbf{\Psi}, \tag{8}$$

where $\mathbf{\Psi} = [sinc(F_s(t - 0/F_s)), \cdots, sinc(F_s(t - K/F_s))]^T$ is given by the Nyquist Theorem as the interpolation matrix from the time domain, and $\mathbf{\Phi}$ is denoted as the recovery matrix from the graph domain.

A. ASSUMPTIONS OF NETWORK STABILITY

Given that most of the network applications work on the stable area, we hereby assume an existence of the equilibrium point $\mathbf{x}_e$ of Eq. (1), and consider the Lyapunov stability of the dynamic graph signals.

Assumption 1: [36] We say $\mathbf{x}(t)$ has the Lyapunov stability on point $\mathbf{x}_e$, if and only if for any $\epsilon > 0$, there exists a $\delta > 0$ such that, if $||\mathbf{x}(0) - \mathbf{x}_e|| < \delta$, then for every $t > 0$ we have

$$||\mathbf{x}(t) - \mathbf{x}_e|| < \epsilon.$$

With the help of the assumption of the Lyapunov stability, the non-linear dynamics of the graph signals can be approximated via the linearized components. We next elaborate the linearizing process and its causing error.

1) LINEARIZE DYNAMICS

Given the Assumption 1, $\mathbf{x}(t)$ converges to $\mathbf{x}_e$, and therefore $\mathbf{x}(\infty) = \mathbf{x}_e$. For convenience, we specify:

$$\mathbf{y}(t) = \mathbf{x}(t) - \mathbf{x}_e, \tag{9}$$

and thus $\lim_{t\to\infty} \mathbf{y}(t) = \mathbf{y}(\infty) = \mathbf{0}$. Then, analyzing the group of nonlinear differential equations in Eq. (1) can be viewed as studying its linear approximations as follows:

$$\begin{aligned} \frac{d\mathbf{y}(t)}{dt} &= \mathbf{J}_f(\mathbf{x}_e) \cdot \mathbf{y}(t) + o\left(\|\mathbf{y}(t)\|\right) + \mathbf{s}(t) \\ &\approx \mathbf{J}_f(\mathbf{x}_e) \cdot \mathbf{y}(t) + \mathbf{s}(t), \end{aligned} \tag{10}$$

where $o\left(\|\mathbf{y}(t)\|\right)$ are terms that go to zeros faster than the first order for $t \to +\infty$. $\mathbf{J}_f(\mathbf{x}_e)$ is the Jacobian matrix of function $f : \mathbb{R}^N \to \mathbb{R}^N$ at $\mathbf{x}_e$, where $f(\cdot)$ is the simplified evolution function of Eq. (1), i.e., $d\mathbf{x}(t)/dt = f(\mathbf{x}(t)) + \mathbf{s}(t)$. $\mathbf{J}_f(\mathbf{x}_e)$ is

computed as:

$$\mathbf{J}_f(\mathbf{x}_e) \triangleq \left[\begin{array}{ccc} \frac{\partial f(t)}{\partial x_1(t)} & \cdots & \frac{\partial f(t)}{\partial x_N(t)} \\ \vdots & \ddots & \vdots \\ \frac{\partial f(t)}{\partial x_1(t)} & \cdots & \frac{\partial f(t)}{\partial x_N(t)} \end{array}\right]\Bigg|_{\mathbf{x}(t)=\mathbf{x}_e}. \quad (11)$$

Further, an intuitive form of Eq, (11) is expressed, as we take Eq. (1) into Eq. (11), i.e.,

$$\mathbf{J}_f(\mathbf{x}_e) = \mathbf{W} \circ \mathbf{J}_G(\mathbf{x}_e) + diag\left\{\frac{\partial F}{\partial x_1}, \cdots, \frac{\partial F}{\partial x_N}\right\}\Bigg|_{\mathbf{x}_e}, \quad (12)$$

where $\circ$ represents the *Hadamard product*, and $\mathbf{J}_G(\mathbf{x}_e)$ is the Jacobian matrix of function $G(\cdot,\cdot)$ at $\mathbf{x}_e$. From Eq. (12), it is observed that $\mathbf{J}_f(\mathbf{x}_e)$ combines both the topology of the network (as is represented by the adjacency matrix $\mathbf{W}$), as well as the dynamic equations (i.e., the mutualistic coupling functions $G(\cdot,\cdot)$ and the self-dynamics $F(\cdot)$ in Eq. (1)).

2) LINEARIZED ERROR

After the derivation of the linearized dynamics, we measure the linearized error via the effectiveness equation [1], [37]. In essence, effectiveness equation of a networked dynamic reduces the N-dimension signals (indexed on N nodes) into 1-dimension. For example, given the signal $\mathbf{y}(t)$, its effectiveness is computed as [1]:

$$\frac{dy_{\text{eff}}(t)}{dt} = \beta_{\text{eff}} \cdot y_{\text{eff}}(t), \quad (13)$$

where $y_{\text{eff}}(t) = \mathbf{1}^T \cdot \mathbf{W} \cdot \mathbf{y}(t)/(\mathbf{1}^T\mathbf{W}\mathbf{1})$, and $\beta_{\text{eff}} = \mathbf{1}^T \cdot \mathbf{W}\mathbf{d}^{\text{in}}$, with the nth entry of $\mathbf{d}^{\text{in}}$ as $d_n = \sum_{m=1}^{N} w_{n,m}$, and $\mathbf{1} \triangleq [1, \cdots, 1]^T$ of size $N \times 1$.

With the help of the 1-dimensional effectiveness $y_{\text{eff}}(t)$ of the N-dimensional $\mathbf{y}(t)$, one can use such effectiveness to measure the linearized error. To be specific, let denote the linearized version of $\mathbf{y}(t)$ in Eq. (10) as $\mathbf{y}_l(t)$, and the linearized error is characterized by the l_1-norm, i.e., $err = \int_0^{+\infty} \|\mathbf{y}_l(t) - \mathbf{y}(t)\|_{l_1} dt$. Then, such error can be measured via the effectiveness error if:

$$c_1 \cdot err \leq \int_0^{+\infty} |y_{\text{l,eff}}(t) - y_{\text{eff}}(t)| dt \leq c_2 \cdot err \quad (14)$$

for some positive constant c_1 and c_2, where $y_{\text{l,eff}}(t) = \mathbf{1}^T\mathbf{W}\mathbf{y}_l(t)/(\mathbf{1}^T\mathbf{W}\mathbf{1})$ can be computed via Eq. (13) with the same Adjacency matrix determined β_{eff}.

We prove Eq. (14) in the following. The right-hand of Eq. (14) is proved by:

$$\begin{aligned} |y_{\text{l,eff}}(t) - y_{\text{eff}}(t)| &= \frac{|\mathbf{1}^T \cdot \mathbf{W}(\mathbf{y}_l(t) - \mathbf{y}(t))|}{|\mathbf{1}^T \cdot \mathbf{W} \cdot \mathbf{1}|} \\ &\leq \frac{\|\mathbf{W}(\mathbf{y}_l(t) - \mathbf{y}(t))\|_{l_1}}{|\mathbf{1}^T \cdot \mathbf{W} \cdot \mathbf{1}|} \\ &\leq \frac{\|\mathbf{W}\|_{l_1}}{|\mathbf{1}^T \cdot \mathbf{W} \cdot \mathbf{1}|} \cdot \|\mathbf{y}_l(t) - \mathbf{y}(t)\|_{l_1}. \end{aligned} \quad (15)$$

The left-hand can be proved by considering the minimum of

$$c(t) = \frac{|y_{\text{l,eff}}(t) - y_{\text{eff}}(t)|}{\|\mathbf{y}_l(t) - \mathbf{y}(t)\|_{l_1}}$$

$$= \frac{1}{|\mathbf{1}^T \cdot \mathbf{W} \cdot \mathbf{1}|} \cdot \frac{|\mathbf{1}^T \cdot \mathbf{W}(\mathbf{y}_l(t) - \mathbf{y}(t))|}{\|\mathbf{y}_l(t) - \mathbf{y}(t)\|_{l_1}}. \quad (16)$$

It is observed from Eq. (16) that the minimal $c(t)$ is zero when $\mathbf{y}_l(t) - \mathbf{y}(t)$ takes from the null-space of $\mathbf{W}$, denoted as $null(\mathbf{W})$. However, $\mathbf{y}_l(t) - \mathbf{y}(t)$ cannot be always the element of $null(\mathbf{W})$ for all $t \in (0, +\infty)$, and therefore there exists some t for $c(t) > 0$. As such, some positive c_1 exist such that the left-hand of Eq. (14) holds.

After the linearization of the non-linear dynamic under the assumption of the Lyapunov stability, we next analyze how to derive the sampling node set, $\mathcal{S}$, the recovery matrix $\mathbf{\Phi}$, and the cut-off frequency Ω_c for these linearized dynamic systems, by analyzing the properties of the Jacobian linearized matrix $\mathbf{J}_f(\mathbf{x}_e)$.

B. GRAPH-DOMAIN BANDLIMITED SIGNALS

With the help of the linearized approximation of the dynamics in Eqs. (10)-(12), we here consider the case where both the initialization $\mathbf{y}(0)$ and the unknown inputs $\mathbf{s}_i$ are $\mathcal{R}$-bandlimited with respect to $\mathbf{J}_f(\mathbf{x}_e)$. In fact, this generally holds for most of the graph signals such as ARMA graph process [30], wave propagations [30], and signal diffusion [30]. The more general cases of initialization and inputs are studied in Section III. C.

1) SAMPLING FROM GRAPH DOMAIN

In order to analyze the graph frequency with respect to $\mathbf{J}_f(\mathbf{x}_e)$, we diagonalize $\mathbf{J}_f(\mathbf{x}_e)$ as:

$$\mathbf{J}_f(\mathbf{x}_e) = \mathbf{U} \cdot diag\{\mu_1, \cdots, \mu_N\} \cdot \mathbf{U}^{-1}, \quad (17)$$

where $\mu_i, i \in \{1, \cdots, N\}$ is the eigenvalues, $\mathbf{U} = [\mathbf{u}_1, \cdots, \mathbf{u}_N]$ is the non-singular matrix composed of the corresponding eigenvectors.

As such, according to Definitions 1-2, the subspace $BL(\mathcal{R}, \mathbf{U}^{-1})$ is constructed and we have $\mathbf{y}(0), \mathbf{s}_i \in BL(\mathcal{R}, \mathbf{U}^{-1})$, given their $\mathcal{R}$-bandlimitedness property. Then, we state that all signals $\mathbf{y}(t) \in BL(\mathcal{R}, \mathbf{U}^{-1})$ by Lemma 1 and Theorem 2, and therefore, the sampling node set $\mathcal{S}$ and the recovery matrix $\mathbf{\Phi}$ can be derived from aforementioned Theorem 1.

Lemma 1: Given $d(\mathbf{y}(t))/dt = \mathbf{J}_f(\mathbf{x}_e) \cdot \mathbf{y}(t)$, if $\mathbf{y}(0) \in BL(\mathcal{R}, \mathbf{U}^{-1})$, then $\mathbf{y}(t) \in BL(\mathcal{R}, \mathbf{U}^{-1})$.

Proof: $\mathbf{y}(t)$ can be computed as

$$\mathbf{y}(t) = e^{t \cdot \mathbf{J}_f(\mathbf{x}_e)} \cdot \mathbf{y}(0). \quad (18)$$

Its graph Fourier transformation with respect to $\mathbf{J}_f(\mathbf{x}_e)$ is:

$$\begin{aligned} \tilde{\mathbf{y}}(t) &= \mathbf{U}^{-1} \cdot e^{t \cdot \mathbf{J}_f(\mathbf{x}_e)} \cdot \mathbf{y}(0) \\ &= \mathbf{U}^{-1} \cdot \sum_{k=0}^{\infty} \frac{t^k}{k!} \cdot \mathbf{J}_f(\mathbf{x}_e)^k \cdot \mathbf{y}(0) \\ &= \sum_{k=0}^{+\infty} \frac{t^k}{k!} \cdot diag\{\mu_1, \cdots, \mu_N\}^k \cdot \mathbf{U}^{-1} \cdot \mathbf{y}(0) \\ &= \sum_{k=0}^{+\infty} \frac{t^k}{k!} \cdot diag\{\mu_1^k, \cdots, \mu_N^k\} \cdot \tilde{\mathbf{y}}(0), \end{aligned} \quad (19)$$

where $\tilde{\mathbf{y}}(0) = \mathbf{U}^{-1} \cdot \mathbf{y}(0)$ and $\mathbf{J}_f(\mathbf{x}_e)^0 = \mathbf{I}_{N\times N}$, the identity matrix of size $N \times N$. This suggests that the subscripts of the non-zero elements of $\tilde{\mathbf{y}}(t)$ coincide with those of $\tilde{\mathbf{y}}(0)$, and therefore all belong to $\mathcal{R}$. Hence, given Definition 2, it proves that $\mathbf{y}(t) \in BL(\mathcal{R}, \mathbf{U}^{-1})$. ■

Theorem 2: Given $d(\mathbf{y}(t))/dt = \mathbf{J}_f(\mathbf{x}_e)\mathbf{y}(t) + \mathbf{s}(t)$, if $\mathbf{y}(0), \mathbf{s}_i = [s_{1,i}, \cdots, s_{N,i}]^T \in BL(\mathcal{R}, \mathbf{U}^{-1})$, then $\mathbf{y}(t) \in BL(\mathcal{R}, \mathbf{U}^{-1})$.

Proof: According to Eq. (2), $\mathbf{s}(t) = \sum_{i=1}^{+\infty} \mathbf{s}_i \circ \boldsymbol{\delta}(t - t_i)$ with $\boldsymbol{\delta}(t - t_i) = [\delta(t - t_i), \cdots, \delta(t - t_i))]^T$ of size $N \times 1$. The proof is equivalent to prove $\mathbf{y}(t) \in BL(\mathcal{R}, \mathbf{U}^{-1})$ for any $t \in [0, t_1) \cup \cdots \cup [t_{+\infty}, +\infty)$. According to Lemma 1, it is proved the $\mathbf{y}(t) \in BL(\mathcal{R}, \mathbf{U}^{-1})$ for any $t \in [0, t_1)$. Then, we notice that $\mathbf{y}(t_1) = e^{t_1 \cdot \mathbf{J}_f(\mathbf{x}_e)} \cdot \mathbf{y}(0) + \mathbf{s}_1$. Thus, if $\mathbf{s}_1 \in BL(\mathcal{R}, \mathbf{U}^{-1})$, then $\mathbf{y}(t_1) \in BL(\mathcal{R}, \mathbf{U}^{-1})$. Taking $\mathbf{y}(t_1)$ as the bandlimited initialization, the proof of $\mathbf{y}(t) \in BL(\mathcal{R}, \mathbf{U}^{-1})$ for interval $t \in [t_1, t_2)$ is straightforward according to Lemma 1. Similarly, we can extend this fact for all the intervals, and therefore prove $\mathbf{y}(t) \in BL(\mathcal{R}, \mathbf{U}^{-1})$. ■

After the proof of $\mathbf{y}(t) \in BL(\mathcal{R}, \mathbf{U}^{-1})$, the sampling method for $\mathbf{y}(t)$ from graph domain can be designed via the existing Theorem 1. To be specific, in order to select the sampling node set $\mathcal{S}$ such that $rank(\mathbf{U}_{\mathcal{SR}}) = |\mathcal{R}|$, one option is to compute $\mathcal{S}$ by finding the maximal $|\mathcal{R}|$ smallest singulars of $\mathbf{U}_{\mathcal{SR}}$, i.e., [18]

$$\mathcal{S} = \underset{\mathcal{S}\subset\mathcal{V}}{\operatorname{argmax}}\, \sigma_{\min}\left(\mathbf{U}_{\mathcal{SR}}\right), \tag{20}$$

where $\sigma_{\min}(\cdot)$ denotes the minimum singular of the matrix. Based on Eq. (20), the recursive *greedy* algorithm can be implemented by finding and adding the row, i.e., $\mathcal{S} \leftarrow \mathcal{S} \cup \{n\}$, such that $n = \operatorname{argmax}_i \sigma_{\min}(\mathbf{U}_{(\mathcal{S}\cup\{i\})\mathcal{R}})$. Then, the recovery matrix $\boldsymbol{\Phi}$ can be computed as $\boldsymbol{\Phi} = \mathbf{U}_{\mathcal{VR}} \cdot (\mathbf{U}_{\mathcal{SR}}^T \cdot \mathbf{U}_{\mathcal{SR}})^{-1} \cdot \mathbf{U}_{\mathcal{SR}}^T$, based on which the recovery process can be pursued as $\hat{\mathbf{y}}(t) = \boldsymbol{\Phi} \cdot \mathbf{y}_{\mathcal{S}}(t)$, with $\mathbf{y}_{\mathcal{S}}(t)$ the sampled signals selected from the sampling node set $\mathcal{S}$.

As such, we determine the sampling node set $\mathcal{S}$ and the recovery matrix that can reconstruct the dynamic graph signals from the graph domain. One major difference between the studies in [30] and our work is that we need to surveillance the sampling node at each discrete time. The reasons is explained as follows. Here, we analyze the linearized dynamics $d\mathbf{y}(t)/dt = \mathbf{J}_f(\mathbf{x}_e)\mathbf{y}(t) + \mathbf{s}(t)$ with the $\mathcal{R}$-bandlimited signals of both the unknown initialization $\mathbf{y}(0)$ and the unknown inputs $\mathbf{s}(t)$. In this view, the overall problem of signal reconstruction cannot be casted equivalently as computing $\mathbf{y}(0)$ from the samples and taking $\mathbf{y}(0)$ into Eq. (18), since we still do not know the exact time and the form of the inputs $\mathbf{s}(t)$. As such, the monitoring of potential inputs requires the samples from $\mathcal{S}$ at each discrete time. Also, such discrete time serves as the fundamental role for discrete-version signals to maintain the characteristics of the continuous networked signals, and we will study how to determine such sampling rate from the time-domain in the following.

2) SAMPLING FROM TIME DOMAIN

After deriving the sampling node set $\mathcal{S}$, and the recovery matrix $\boldsymbol{\Phi}$, we will deduce the time-domain cut-off frequency Ω_c via Lemma 2 and Theorem 3.

Lemma 2: Consider $d\mathbf{y}(t)/dt = \mathbf{J}_f(\mathbf{x}_e)\mathbf{y}(t)$ satisfying Lyapunov stability. Given that we are only interested in frequency components of time-domain larger than a threshold ε, the time-domain cut-off frequency Ω_c can be computed as:

$$\Omega_c = \max_{j\in\mathcal{R}} \left|\mathrm{Im}[\mu_j]\right| + \sqrt{\frac{\|\mathbf{y}(0)\|_2^2}{\varepsilon^2} - \min_{j\in\mathcal{R}} \mathrm{Re}[\mu_j]^2}. \tag{21}$$

Proof: According to Eq. (18), each $y_n(t)$ of $\mathbf{y}(t)$ can be expressed as:

$$y_n(t) = \sum_{j\in\mathcal{R}} u_{n,j} \cdot \tilde{y}_j(0) \cdot e^{\mu_j t}, \tag{22}$$

where $u_{i,j}$ is the entry of $\mathbf{U}$. Given that $\mathbf{y}(t)$ is Lyapunov stable, the eigenvalues of $\mathbf{J}_f(\mathbf{x}_e)$ have non-positive real values [36], i.e., $\mathrm{Re}[\mu_j] \le 0$. Hence, the time-frequency Fourier transform of $y_n(t)$ is computed as:

$$\begin{aligned} Y_n(\Omega) &= \int_0^{+\infty} \sum_{j\in\mathcal{R}} u_{n,j} \cdot \tilde{y}_j(0) \cdot e^{\mu_j t} \cdot e^{-i\Omega t} dt \\ &= \sum_{j\in\mathcal{R}} u_{n,j} \cdot \tilde{y}_j(0) \int_0^{+\infty} e^{\mathrm{Re}[\mu_j]t - i(\Omega - \mathrm{Im}[\mu_j])t} dt \\ &= \sum_{j\in\mathcal{R}} \frac{u_{n,j} \cdot \tilde{y}_j(0)}{-\mathrm{Re}[\mu_j] + i\left(\Omega - \mathrm{Im}[\mu_j]\right)}. \end{aligned} \tag{23}$$

The magnitude of $Y_n(\Omega)$ is computed as:

$$\begin{aligned} |Y_n(\Omega)| &= \left| \sum_{j\in\mathcal{R}} \frac{u_{n,j} \cdot \tilde{y}_j(0)}{-\mathrm{Re}[\mu_j] + i\left(\Omega - \mathrm{Im}[\mu_j]\right)} \right| \\ &\le \sum_{j\in\mathcal{R}} \left| \frac{u_{n,j} \cdot \tilde{y}_j(0)}{-\mathrm{Re}[\mu_j] + i\left(\Omega - \mathrm{Im}[\mu_j]\right)} \right| \\ &\le \sum_{j\in\mathcal{R}} \frac{|u_{n,j} \cdot \tilde{y}_j(0)|}{\sqrt{\mathrm{Re}^2[\mu_j] + \left(\Omega - \mathrm{Im}(\mu_j)\right)^2}}. \end{aligned} \tag{24}$$

We can learn from Eq. (24) that the imaginary parts of the eigenvalues contribute to the left/right shift of Ω. Hence, for any $\Omega > \max_{j\in\mathcal{R}} \left|\mathrm{Im}[\mu_j]\right|$, we have:

$$\begin{aligned} |Y_n(\Omega)| &< \frac{\sum_{j=1}^N |u_{n,j} \cdot \tilde{y}_j(0)|}{\sqrt{\min_{j\in\mathcal{R}} \mathrm{Re}[\mu_j]^2 + \left(\Omega - \max_{j\in\mathcal{R}} \left|\mathrm{Im}[\mu_j]\right|\right)^2}} \\ &< \frac{\sqrt{\sum_{j=1}^N u_{n,j}^2 \sum_{j=1}^N \tilde{y}_j(0)^2}}{\sqrt{\min_{j\in\mathcal{R}} \mathrm{Re}[\mu_j]^2 + \left(\Omega - \max_{j\in\mathcal{R}} \left|\mathrm{Im}[\mu_j]\right|\right)^2}} \end{aligned}$$

$$= \frac{\|\tilde{\mathbf{y}}(0)\|_2}{\sqrt{\min_{j\in\mathcal{R}}\mathrm{Re}[\mu_j]^2 + \left(\Omega - \max_{j\in\mathcal{R}}\left|\mathrm{Im}[\mu_j]\right|\right)^2}}$$
$$= \frac{\|\mathbf{U}\cdot\tilde{\mathbf{y}}(0)\|_2}{\sqrt{\min_{j\in\mathcal{R}}\mathrm{Re}[\mu_j]^2 + \left(\Omega - \max_{j\in\mathcal{R}}\left|\mathrm{Im}[\mu_j]\right|\right)^2}}$$
$$= \frac{\|\mathbf{y}(0)\|_2}{\sqrt{\min_{j\in\mathcal{R}}\mathrm{Re}[\mu_j]^2 + \left(\Omega - \max_{j\in\mathcal{R}}\left|\mathrm{Im}[\mu_j]\right|\right)^2}}. \quad (25)$$

Then, by making the right-hand of Eq. (25) smaller than ε, we derive the cut-off frequency Ω_c given by Lemma 2. ■

Theorem 3: Given $d\mathbf{y}(t)/dt = \mathbf{J}_f(\mathbf{x}_e)\mathbf{y}(t) + \mathbf{s}(t)$ satisfying Lyapunov stability, the time-domain cut-off frequency Ω_c can be computed as:

$$\Omega_c = \max_{j\in\mathcal{R}}\left|\mathrm{Im}[\mu_j]\right| + \sqrt{\frac{\|\mathbf{y}(0)\|_2^2 + \sum_i \|\mathbf{s}_i\|_2^2}{\varepsilon^2} - \min_{j\in\mathcal{R}}\mathrm{Re}[\mu_j]^2}. \quad (26)$$

Proof: According to Lemma 2, the Fourier-transform of $\mathbf{y}(t)$ is the summation of Eq. (23) with different inputs $\mathbf{s}_i$. As such, the magnitude of $Y_n(\Omega)$ is

$$|Y_n(\Omega)| < \frac{\|\mathbf{y}(0)\|_2 + \sum_i \|\mathbf{s}_i\|_2}{\sqrt{\min_{j\in\mathcal{R}}\mathrm{Re}[\mu_j]^2 + \left(\Omega - \max_{j\in\mathcal{R}}\left|\mathrm{Im}[\mu_j]\right|\right)^2}}. \quad (27)$$

By making the right-hand of Eq. (27) smaller than ε, we prove Theorem 3. ■

With the help of Theorem 3, we compute the cut-off frequency Ω_c, which can be used to determine the sampling rate to discretize the continuous graph signals. Also, one can resort to the Shannon sampling interpolation in Eqs. (7)-(8) to verify the rationality of such computed Ω_c.

C. GENERAL CASE WITH ARBITRARY INITIALIZATION

It is noteworthy that the $\mathcal{R}$-bandlimited property of the initialization and the inputs may not be easily satisfied for some monitoring tasks. Such $\mathbf{y}(0), \mathbf{s}_i \notin BL(\mathcal{R}, \mathbf{U}^{-1})$ renders difficulties for monitoring the graph signals, as the operator $\mathbf{J}_f(\mathbf{x}_e)$ cannot maintain the $\mathcal{R}$-bandlimitedness of the signal $\mathbf{y}(t)$, thereby making the computation of reliable $\mathcal{S}$ and Ω_c challenging. Here, inspired by the sampling theories deduced with the bandlimited signals, we provide an imperfect sampling method for this case from both the time and graph -domain.

From the perspective of graph-domain sampling, an intuitive idea is to select the subscripts of the $|\mathcal{S}|$ smallest magnitudes of real parts of eigenvalues as $\mathcal{R}$, and regard $\mathbf{y}(0)$ and $\mathbf{s}_i$ as the approximated $\mathcal{R}$-bandlimited signals. We explain the reason in the following. According to Eq. (19), the graph Fourier transformation of $\mathbf{y}(t)$ for jth graph-frequency component is:

$$\tilde{y}_j(t) = e^{\mu_j\cdot t}\tilde{y}_j(0) + \sum_{t_i\le t} e^{\mu_j\cdot(t-t_i)}\tilde{s}_{j,i}, \quad (28)$$

based on which the energy in terms of the integral with respect to t can be computed as:

$$E_j = \int_0^{+\infty} |\tilde{y}_j(t)|dt = \frac{|\tilde{y}_j(0) + \sum_i \tilde{s}_{j,i}|}{|\mathrm{Re}[\mu_j]|}, \quad (29)$$

where $\mathrm{Re}[\mu_j] < 0$ according to the Lypunov stability assumption. As such, given the randomness of both $\mathbf{y}(0)$ and $\mathbf{s}_i$, one option is to minimize the energies of the un-selected graph-frequency parts, and thereby we neglect the $N - |S|$ largest $|\mathrm{Re}[\mu_j]|$. According to Eq. (29), the reconstructed error is computed as follows:

$$\int_0^{+\infty} \|\hat{\mathbf{y}}(t) - \mathbf{y}(t)\|_2 dt \le \frac{\|\mathbf{y}(0)\|_2 + \sum_i \|\mathbf{s}_i\|_2}{|\mathrm{Re}[\mu]|} \cdot \frac{N - |\mathcal{S}|}{N}. \quad (30)$$

where $|\mathrm{Re}(\mu)|$ represents the $|\mathcal{S}| + 1$ smallest $|\mathrm{Re}(\mu_n)|$ for $n \in \{1, \cdots, N\}$.

We then analyze the time-domain sampling. Given that as $\mathbf{y}(0)$ and $\mathbf{s}_i$ are not $\mathcal{R}$-bandlimited with respect to $\mathbf{J}_f(\mathbf{x}_e)$, the sampling theory from Theorem 3 cannot hold, since all the eigenvalues of $\mathbf{J}_f(\mathbf{x}_e)$ contribute to the cut-off frequency Ω_c. As such, a similar form of cut-off frequency Ω_c from the time-domain is obtained by changing the range of eigenvalues' indices of Theorem 3 to following equations, i.e.,

$$\Omega_c = \max_{j\in\{1,\cdots,N\}}\{\left|\mathrm{Im}[\mu_j]\right|\} + \sqrt{\frac{\|\mathbf{y}(0)\|_2^2 + \sum_i \|\mathbf{s}_i\|_2^2}{\varepsilon^2} - \min_{j\in\{1,\cdots,N\}}\{\mathrm{Re}[\mu_j]\}^2}. \quad (31)$$

As such, we derive the graph-domain sampling node set $\mathcal{S}$, and time-domain cut-off frequency Ω_c, for any unknown arbitrary initialization and inputs.

D. EXPLICIT RELATIONSHIP BETWEEN OPTIMAL SAMPLING AND GRAPH DYNAMICS

It is important to stress that a key benefit of our framework is the creation of an **explicit relationship** between the time- and graph-domain cut-off frequencies, the graph properties, and the nonlinear dynamics. We will elaborate this relationship from three aspects.

(i) The networked dynamics characterized by the self-dynamic function and the mutualistic coupling equations in Eq. (1) is interpreted by the linearized matrix $\mathbf{J}_f(\mathbf{x}_e)$ from Eq. (10). For example, the stability of the network can be analyzed via the real parts of the eigenvalues of $\mathbf{J}_f(\mathbf{x}_e)$ (seen from Fig. 3(a)).

(ii) In the case of the graph-domain $\mathcal{R}$-bandlimited initialization and inputs with respect to $\mathbf{J}_f(\mathbf{x}_e)$, it is proved from Theorem 2 that $\mathbf{y}(t) \in BL(\mathcal{R}, \mathbf{U}^{-1})$, and therefore the graph non-zero frequency indices of $\mathbf{y}(t)$ compose the set $\mathcal{R}$. This $\mathcal{R}$ further maps the eigenvalues (graph-domain frequencies) illustrated in Fig. 3(a), such that only the bases (eigenvectors)

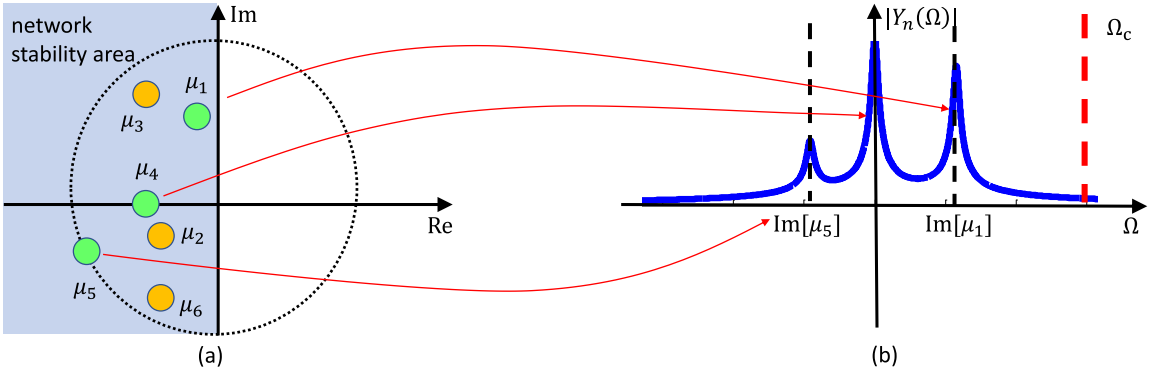

FIGURE 3. Illustration of the relations between graph-domain band-set $\mathcal{R} = \{1, 4, 5\}$, the time-domain cut-off frequency Ω_c, and the underlying graph structure and its governing nonlinear dynamics $\mathbf{J}_f(\mathbf{x}_e)$. Subplots: (a) network stability area for the eigenvalues of $\mathbf{J}_f(\mathbf{x}_e)$, which is also the graph-domain frequencies whose subscripts belong to $\mathcal{R}$; and (b) the magnitude of time-frequency Fourier transform $|Y_n(\Omega)|$ for the graph-domain $\mathcal{R}$-bandlimited signals. It can be seen that the eigenvalues of $\mathbf{J}_f(\mathbf{x}_e)$ whose subscripts belong to $\mathcal{R}$ (i.e., μ_1, μ_4, μ_5) determines the shape of $|Y_n(\Omega)|$. This further demonstrates that the time-domain cut-off frequency Ω_c can be determined by Theorem 3.

whose subscripts of eigenvalues belongs to $\mathcal{R}$ have non-zero coefficients.

(iii) This graph-domain bandlimited set $\mathcal{R}$ further leads to the computation of the time-domain cut-off frequency, as only the subscripts of eigenvalues of $\mathbf{J}_f(\mathbf{x}_e)$ that belongs to $\mathcal{R}$ affect the shape of the time-frequency Fourier transform (seen from Fig. 3(b)). Specially, a direct relation of Ω_c and $\mathcal{R}$ is shown in Theorem 3. In summary, as is illustrated in Fig. 3, we can see that the time-domain cut-off frequency Ω_c is related to the eigenvalues whose subscripts belong to $\mathcal{R}$, which in turn is related to the optimally sampled graph structure and the underlying dynamics.

IV. SIMULATIONS

In the following analysis, the performance of our proposed sample theory will be evaluated. First, we examine the performance in the case when the unknown $\mathbf{y}(0)$ and $\mathbf{s}_i$ are $\mathcal{R}$-bandlimited with respect to $\mathbf{J}_f(\mathbf{x}_e)$. Then, the general cases in which $\mathbf{y}(0), \mathbf{s}_i \notin BL(\mathcal{R}, \mathbf{U}^{-1})$ is evaluated. To do so, we specify the root mean square error (RMSE) of $\hat{\mathbf{x}}(t), t \in [0, T]$, i.e.,

$$\begin{aligned}\mathrm{RMSE} &= \mathbb{E}\{\hat{\mathbf{x}}(t) - \mathbf{x}(t)\} \\ &\backsimeq \sqrt{\frac{\Delta_t}{NT}\sum_{k=0}^{T/\Delta_t - 1} \|\hat{\mathbf{x}}(k\Delta_t) - \mathbf{x}(k\Delta_t)\|_2^2}, \quad (32)\end{aligned}$$

where Δ_t is the sample rate whose corresponding time-domain frequency is much greater than the cut-off frequency, i.e., $1/\Delta_t = 4\Omega_c/\pi$.

Note that in this simulation, it is difficult to provide any comparison with existing sampling methods, as most of the referenced works (e.g., [25], [30]) concentrated on discrete-time graph process rather than continuous signals. In addition, their works prefer the dynamic sampling set selections varying with the time, which may not be suitable for sensor placement requiring fixed sampling node set $\mathcal{S}$ for sensor deployment.

As such, we just make a comparison with their works by stating the differences. For the study in [25], the author designed a joint Fourier-Graph sampling method, by using the topology-based Laplacian operator, and the Discrete Fourier Transform (DFT) matrix. The difference lies in that they did not consider how to maintain an $\mathcal{R}$-bandlimited property for the time-varying graph signals, and therefore cannot obtain a fixed sampling node set for sensor placement. For the study in [30], the sequential Kalman filter was designed to track the discrete graph signals under the assumptions of known inputs. However, such scheme cannot address the unknown inputs challenges, as the unknown inputs lead to the unavailability of the transitional probability density function, which blocks the predict-stage of current state from the last state. More importantly, they did not analyze the case when the initialization and the inputs are not $\mathcal{R}$-bandlimited (as what we do in Section III. C).

For this simulation, the involved dynamic functions are configured as follows. As far as both the linear and nonlinear dynamic networks are concerned, we consider two types of dynamic models [3]:

$$\frac{dx_n(t)}{dt} = -Bx_n(t) + R\sum_{m=1}^{N} w_{n,m}x_m(t) + \sum_{i=1}^{+\infty} s_{n,i}\delta(t - t_i), \quad (33)$$

$$\begin{aligned}\frac{dx_n(t)}{dt} &= F - Bx_n(t) + R\sum_{m=1}^{N} w_{n,m} \cdot x_n(t) \cdot x_m(t) \\ &\quad + \sum_{i=1}^{+\infty} s_{n,i} \cdot \delta(t - t_i). \quad (34)\end{aligned}$$

Eq. (33) is referred as the linear population dynamics (PD) model, where each node's population has a self growth rate $-B$ and also depends on the migration strength R from neighbouring connected nodes. Eq. (34) is referred as the non-linear protein interaction model that describes the nonlinear dynamics of protein-protein interactions captured by mass-action kinetics (MAK). The detailed parameters and explanations for the differential equations are found

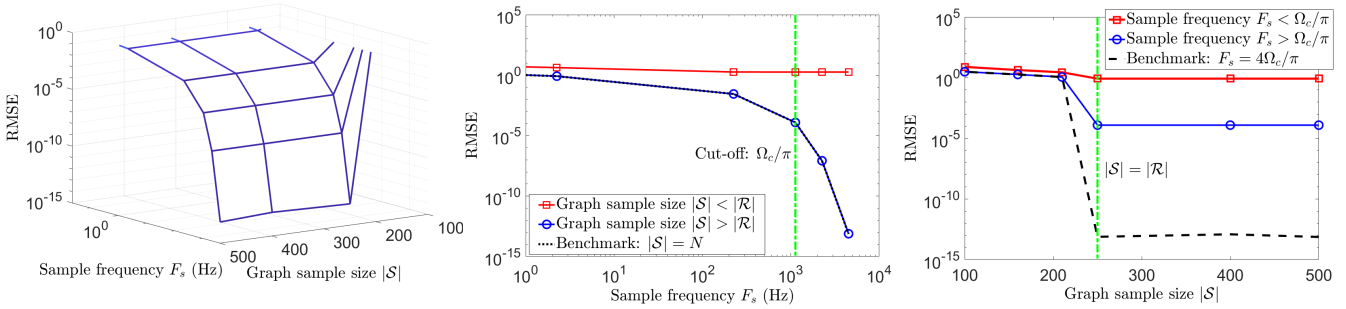

FIGURE 4. Performance of the sampling theory on PD linear dynamic network with bandlimited initialization and inputs: (a) RMSE with respect to both the sample frequency F_s and the graph sample size $|\mathcal{S}|$, (b) illustrates one tangent plane of (a), RMSE related to the sample frequency F_s with fixed graph sample size $|\mathcal{S}|$, and (c) shows another tangent plane, the RMSE affected by only the graph sample size $|\mathcal{S}|$.

in [3]. In Eqs. (33)-(34), we assign the number of nodes $N = 500$, and leave other parameters randomly configured such that they satisfy the Lypunov stability assumed in Assumption 1.

A. PERFORMANCE WITH BANDLIMITED INITIALIZATION

We first evaluate the performance for the graph-domain bandlimited initialization and inputs by studying the RMSE in both the linear model and the nonlinear model.

1) LINEAR MODEL

We illustrate the performance of the sampling theory via the combining time- and graph- domains from Fig. 4. Fig. 4(a) provides the RMSE with respect to the joint time-domain sample frequency F_s and the graph sample size $|\mathcal{S}|$. We can see that with the increases of both F_s and $|\mathcal{S}|$, the RMSE decreases, suggesting that the performance of recovering the dynamic graph signals improves, as more samples from both the time- and the graph- domains are involved. This can be also demonstrated in Fig. 4(b) and Fig. 4(c), whereby the two tangent planes of Fig. 4(a) are given.

Fig. 4(b) investigates the changes of the RMSEs that varied by the time-domain sample frequency F_s, as the various fixed graph sample sizes $|\mathcal{S}|$ are considered. With the growth of F_s, the RMSEs are decreasing. Also, it compares the cases whether the fixed graph sample size is larger than the cut-off graph sample size, i.e., $|\mathcal{S}| \gtrless |\mathcal{R}|$. In the case of $|\mathcal{S}| > |\mathcal{R}|$, the RMSE decreases from 10^{-1} to 10^{-15} as F_s grows from 10^0 to 10^{-4}. This is because that, an increase of time-domain sample frequency F_s means a growth number of samples from the time-domain, which improves the performance of recovery, according to the Nyquist sample theory. It is also noteworthy that the RMSE from a graph sample size no lesser than the cut-off graph sample size i.e., $|\mathcal{S}| \geq |\mathcal{R}|$ equals to the Benchmark whereby all the nodes are sampled i.e., $|\mathcal{S}| = N$. This is because that in a linear model e.g., the PD model, a perfect recovery can be achieved as $rank\,(\mathbf{U}_{\mathcal{SR}}) = |\mathcal{R}|$ is reaching. Then, we consider the case where $|\mathcal{S}| < |\mathcal{R}|$. We can observe that the RMSE decreases little with the growth of the time-domain sample frequency F_s, as the perfect recovery cannot be realized if graph sample size is smaller than $|\mathcal{R}|$.

Fig. 4(c) illustrates the RMSEs with respect to the graph sample size $|\mathcal{S}|$ with the fixed time-domain sample frequencies. As aforementioned. we can firstly observe that the RMSEs decrease with the growth of $|\mathcal{S}|$. Then, we can see that the RMSE from the case $F_s > \Omega_c/\pi$ is lower as opposed to that from $F_s < \Omega_c/\pi$, since the recovery performance of the latter case are deteriorated by the lack of samples from time-domain. Also, the threshold ε of the magnitude of the frequency transform from Theorem 3 matters, as the computation process of the cut-off frequency Ω_c neglects the frequency parts whose magnitudes are smaller than the threshold. This leads to the gap between the benchmark with a larger $F_s = 4\Omega_c/\pi$ and the RMSE whose $F_s = \Omega_c/\pi$. Furthermore, we can notice that, after the graph sample size reaches the size of $\mathcal{R}$ i.e., $|\mathcal{S}| = |\mathcal{R}|$ the RMSEs converges to a limitation. The reason can be categorized as that, in the case of a linear model such as the PD model, Theorem 2 holds true. In other words, if the initialization and the inputs are $\mathcal{R}$-bandlimited with respect to $\mathbf{J}_f(\mathbf{x}_e)$ (i.e., $\mathbf{y}(0), \mathbf{s}_i \in BL(\mathcal{R}, \mathbf{U}^{-1})$), then $\mathbf{y}(t) \in BL(\mathcal{R}, \mathbf{U}^{-1})$, which suggests that we can use any $\mathcal{S}$ as a sampling set such that $rank\,(\mathbf{U}_{\mathcal{SR}}) = |\mathcal{R}|$, and the signals can be perfectly recovered.

2) NONLINEAR MODEL

The performance of the sampling theory via the joint time- and graph- domains is illustrated from Fig. 5. Fig. 5(a) shows the RMSE with respect to both the time-domain sample frequency F_s and the graph sample size $|\mathcal{S}|$. It is intuitive that as F_s and $|\mathcal{S}|$ increase, the RMSE keeps decreasing, which suggests that the recovery of dynamic graph signals become better as more samples are considered. This can be also demonstrated in Fig. 5(b) and Fig. 5(c), whereby the two tangent planes of Fig. 5(a) are provided.

Fig. 5(b) illustrates RMSEs that are influenced only by the time-domain sample frequency F_s, as we fix the graph sample size $|\mathcal{S}|$. We can observe that with the increase of F_s, the RMSEs are decreasing. Moreover, it compares the cases whether the fixed graph sample size is larger than the cut-off graph sample size, i.e., $|\mathcal{S}| \gtrless |\mathcal{R}|$. For the case $|\mathcal{S}| > |\mathcal{R}|$, the RMSE decreases at first (from 10^{-1} to 10^{-5}), and then converges to a limit (as 10^{-5}), which is different

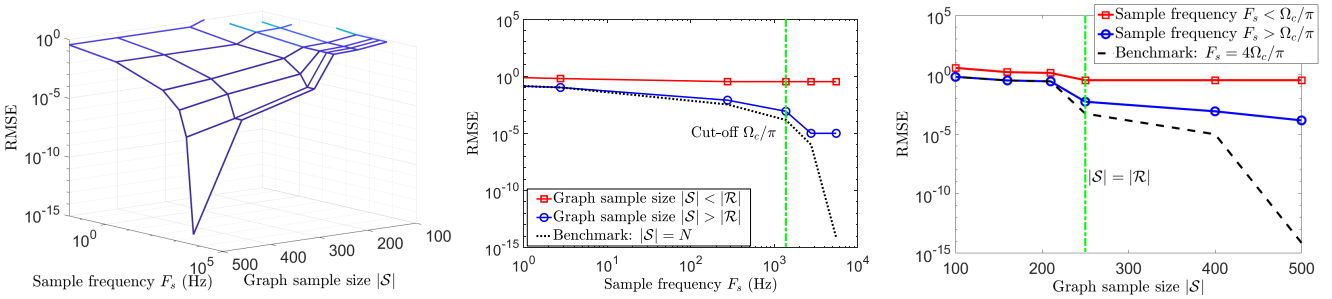

FIGURE 5. Performance of the sampling theory on MAK nonlinear dynamic network with bandlimited initialization and inputs: (a) RMSE with respect to both the sample frequency F_s and the graph sample size $|\mathcal{S}|$, (b) illustrates the tangent plane of (a), RMSE corresponding to the sample frequency F_s as the graph sample size $|\mathcal{S}|$ is fixed, and (c) gives another tangent plane, the RMSE influenced by only the effect of graph sample size $|\mathcal{S}|$.

from Fig. 4(b). The reasons are given as follows. Firstly, as the time-domain sample frequency F_s becomes larger, the performance of recovery improves given by the Nyquist sample theory. Then, given the linear approximation of the nonlinear network in Eq. (10), there exists an error limitation measured by Eq. (14), which cannot be surpassed only by increasing F_s. This limitation (computed as $10^{-5} - 10^{-15}$) is illustrated by the benchmark in Fig. 5(b) that uses samples of all the nodes from the graph i.e., $|\mathcal{S}| = N$. It is also noteworthy that after F_s surpasses the cut-off frequency Ω_c/π, the RMSE are still decreasing. This is because the computation of Ω_c from Theorem 3 ignore the frequency parts whose amplitudes are smaller that the threshold ε. Also, we consider the case where $|\mathcal{S}| < |\mathcal{R}|$. We can observe that the RMSE decreases little as the sample frequency grows. This is because if graph sample size is small, we cannot recover the signals for all N nodes, which limits the RMSE from being decreased.

Fig. 5(c) gives the RMSEs with respect to the graph sample size $|\mathcal{S}|$ via the fixed time-domain sample frequencies. As aforementioned, the RMSEs decrease with the growth of $|\mathcal{S}|$. Then, we can see that the RMSE from the case $F_s > \Omega_c/\pi$ outperforms the one of $F_s < \Omega_c/\pi$, as the error from the latter case are restricted by the lack of samples from the time-domain. Also, the threshold of the magnitude of the frequency transform from Theorem 3 matters, as the computed cut-off frequency Ω_c ignores those whose amplitudes are lesser than the threshold. This gives rise to the gap between the benchmark with a larger $F_s = 4\Omega_c/\pi$ and the RMSE whose $F_s = \Omega_c/\pi$. In addition, we can notice that unlike Fig. 4(c) where the RMSEs converges to a limitation after the graph sample size is greater than the cut-off sample size i.e., $|\mathcal{S}| \geq |\mathcal{R}|$, the RMSEs are still decreasing. The reason can be categorized as that, the graph sample theory we deduced in Theorem 2 is based on the linear system. It is true that Theorem 2 is still suitable for the nonlinear cases if their dynamic functions satisfy the Lyapunov stability, but the high-order term in Eq. (10) yields the error unless all the nodes from the graph are sampled, i.e., $|\mathcal{S}| = N$. Also, this error gap can be demonstrated and computed via the Benchmark whose sample size is $|\mathcal{S}| = N$.

B. PERFORMANCE WITH ARBITRARY INITIALIZATION

We then examine our proposed sampling method for arbitrary initialization and inputs via the nonlinear model of Eq. (34). The performance of signal recovery is shown in Fig. 6. Fig. 6(a) provides the RMSE varying with both the time-domain sample frequency F_s and the graph sample size $|\mathcal{S}|$. Similar to the bandlimited cases, the RMSE decreases as F_s and $|\mathcal{S}|$ increase, demonstrating a higher successful recovery of dynamic graph can be achieved, as more samples are applied.

Fig. 6(b) illustrates RMSEs with respect to only the time-domain sample frequency F_s, as fixed the graph sample sizes are considered. It is observed that with the increase of F_s, the RMSEs are decreasing. Then, it gives the result of comparison between different graph sample sizes, i.e., $|\mathcal{S}| = 4N/5$ and $|\mathcal{S}| = 2N/5$. We can easily see that the graph sample size $|\mathcal{S}|$ serves as the basic condition for the performance of recovery. This is because if graph sample size is small (i.e., $|\mathcal{S}| = 2N/5$), we cannot recover the signals for all N nodes, rendering the RMSE as a constant. Furthermore, we analyze the case with larger graph sample size, i.e., $|\mathcal{S}| = 4N/5$. We can observe that the RMSE decreases at first (from 10^{-1} to 10^{-2}), and then converges to a limit (as 10^{-2}), which is higher than that from Fig. 5(b). The reasons can be categorized as follows. Firstly, just like the bandlimited cases, the performance of recovery improves with a larger time-domain sample frequency F_s, and the aforementioned limitation of the linear approximation contributes to its convergence. Second, different from the bandlimited cases, we select $|\mathcal{S}|$ smallest magnitudes of real parts of eigenvalues as $\mathcal{R}$, and regard $\mathbf{y}(0)$ and $\mathbf{s}_i$ as the approximated $\mathcal{R}$-bandlimited signals. In this view, an error is inevitable as we neglect parts of the dynamics when sampling and recovering the signals (as is shown in Eq. (30)). This limitation (computed as $10^{-2} - 10^{-15}$) is illustrated by the benchmark in Fig. 6(b) that uses samples from all the nodes from the graph i.e., $|\mathcal{S}| = N$. We should also note that after F_s surpasses the cut-off frequency Ω_c/π, the RMSE are still decreasing. This is because the computation of Ω_c from Eq. (31) ignore the frequency components whose magnitudes are smaller that the threshold ε.

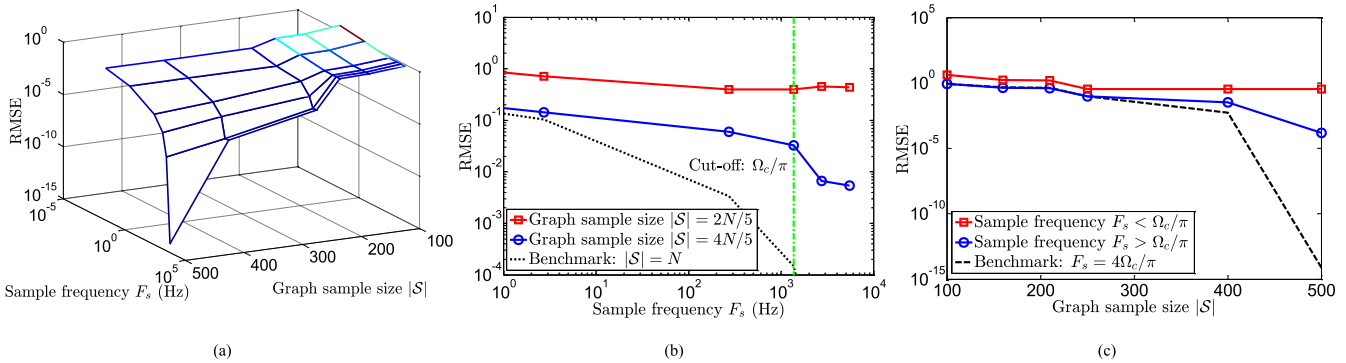

FIGURE 6. Performance of the sampling theory on MAK nonlinear dynamic network with arbitrary initialization and inputs: (a) RMSE with respect to both the sample frequency F_s and the graph sample size $|\mathcal{S}|$, (b) illustrates one tangent plane of (a), RMSE related to the sample frequency F_s with fixed graph sample size $|\mathcal{S}|$, and (c) shows another tangent plane, the RMSE affected by only the graph sample size $|\mathcal{S}|$.

Fig. 6(c) illustrates the RMSEs with respect to the graph sample size $|\mathcal{S}|$ where the time-domain sample frequencies F_s are fixed. As aforementioned, the RMSEs decrease with the growth of $|\mathcal{S}|$. Yet the reason is not only the linear approximation as the bandlimited cases have, the approximation of arbitrary initialization and inputs to the bandlimited one in Section III. C matters, since we ignore the $N - |\mathcal{S}|$ minimum energies in Eq. (29) from the graph frequency domain. Then, we can see that the RMSE from the case $F_s > \Omega_c/\pi$ outperforms that of $F_s < \Omega_c/\pi$, since the error from the latter case are restricted by the lack of samples from time-domain. Also, the gap between the benchmark with a larger $F_s = 4\Omega_c/\pi$ and the RMSE whose $F_s = \Omega_c/\pi$ is obvious. This is mainly because the computation of the cut-off frequency Ω_c ignores the parts whose magnitudes are lesser than the threshold.

V. CONCLUSION & FUTURE RESEARCH

In this paper, we developed a theory for the time- and graph-domain joint sampling of a networked dynamical system with unknown bandlimited initialization and inputs in the graph spectral domain. We first interpret the networked dynamics into a linearized matrix, from which the stability of the network can be analyzed via its eigenvalues. Then, We prove that the dynamic signals can be sampled and fully recovered if the network are stable and their initialization and inputs are bandlimited with respect to the matrix.

Unlike other high-dimensional data sets, we consider dynamical graphs with nonlinear dynamics that have explicit causal relations between nodes. Therefore, our sampling theory is able to directly map optimal graph sampling locations and rates to the graph properties and governing nonlinear dynamics. Changes in the underlying dynamics or the network structure will be able to directly inform the optimal data sampling process (see Fig. 3). Together with recent advances in understanding how topology interacts with dynamics [1], [13], we now understand how the aforementioned factors influence both time- and graph-domain information sampling.

The application domains extend across many engineering, social, and biological complex systems, and we demonstrate our theory on a linear population dynamic (PD) model and a non-linear protein interaction (MAK) model. For recovering the dynamics, our results show that the RMSE drop dramatically by several orders of magnitude when we sample above the optimal sampling rate.

The limitation of our work thus far as been on studying first order one-dimensional Markovian nonlinear dynamics and bandlimited initialization and inputs. Many complex systems are a multiplex of different network and dynamics (e.g. multiplexed transport networks [38]), with dynamics in at least two-dimensions with higher order differential equations (e.g. water distribution networks [39] and electricity supply networks [7]), and have non-Markovian dynamics (e.g. have extended memory of epidemic networks [10]). Extending our framework to such network dynamics will be the focus of our future work.

Author Contributions & Declarations: Z.W. developed the theory and conducted the simulations. W.G. developed the idea and suggested the case studies. B.L., Z.W. and W.G. jointly wrote the paper. The authors have no conflict of interests.

REFERENCES

[1] J. Gao, B. Barzel, and A.-L. Barabási, "Universal resilience patterns in complex networks," *Nature*, vol. 530, no. 7590, pp. 307–312, Feb. 2016.

[2] S. Krishnagopal, J. Lehnert, W. Poel, A. Zakharova, and E. Schöll, "Synchronization patterns: From network motifs to hierarchical networks," *Philos. Trans. Roy. Soc. A, Math. Phys. Eng. Sci.*, vol. 375, no. 2088, Mar. 2017, Art. no. 20160216.

[3] B. Barzel and A.-L. Barabási, "Universality in network dynamics," *Nature Phys.*, vol. 9, no. 10, pp. 673–681, Sep. 2013.

[4] A. Wilson, "Boltzmann, lotka and volterra and spatial structural evolution: An integrated methodology for some dynamical systems," *J. Roy. Soc. Interface*, vol. 5, no. 25, pp. 865–871, Dec. 2007.

[5] S. Dhamal, R. D. Vallam, and Y. Narahari, "Modeling spread of preferences in social networks for sampling-based preference aggregation," *IEEE Trans. Netw. Sci. Eng.*, vol. 6, no. 1, pp. 46–59, Jan./Mar. 2019.

[6] M. Bardoscia, S. Battiston, F. Caccioli, and G. Caldarelli, "Pathways towards instability in financial networks," *Nature Commun.*, vol. 8, Feb. 2017, Art. no. 14416.

[7] B. Schäfer, D. Witthaut, M. Timme, and V. Latora, "Dynamically induced cascading failures in power grids," *Nature Commun.*, vol. 9, no. 1, May 2018, Art. no. 1975.

[8] X. Lu, C. Gray, L. E. Brown, M. E. Ledger, A. M. Milner, R. J. Mondragón, G. Woodward, and A. Ma, "Drought rewires the cores of food webs," *Nature Climate Change*, vol. 6, no. 9, pp. 875–878, May 2016.

[9] Y. Hasegawa, "Thermodynamics of collective enhancement of precision," *Phys. Rev. E, Stat. Phys. Plasmas Fluids Relat. Interdiscip. Top.*, vol. 98, no. 3, Sep. 2018, Art. no. 032405.

[10] I. Scholtes, N. Wider, R. Pfitzner, A. Garas, C. J. Tessone, and F. Schweitzer, "Causality-driven slow-down and speed-up of diffusion in non-Markovian temporal networks," *Nature Commun.*, vol. 5, Sep. 2014, Art. no. 5024.

[11] C. Ellinas, N. Allan, and A. Johansson, "Dynamics of organizational culture: Individual beliefs vs. social conformity," *PLoS One*, vol. 12, no. 6, Jun. 2017, Art. no. e0180193.

[12] M. F. Duarte, G. Shen, A. Ortega, and R. G. Baraniuk, "Signal compression in wireless sensor networks," *Philos. Trans. Roy. Soc. A, Math., Phys. Eng. Sci.*, vol. 370, no. 1958, pp. 118–135, Jan. 2012.

[13] C. Hens, U. Harush, S. Haber, R. Cohen, and B. Barzel, "Spatiotemporal signal propagation in complex networks," *Nature Phys.*, vol. 15, pp. 403–412, Jan. 2019.

[14] F. R. Chung and F. C. Graham, *Spectral Graph Theory*, no. 92. Providence, RI, USA: American Mathematical Society, 1997.

[15] I. Pesenson, "Sampling in paley-wiener spaces on combinatorial graphs," *Trans. Amer. Math. Soc.*, vol. 360, no. 10, pp. 5603–5627, 2008.

[16] A. Sandryhaila and J. M. F. Moura, "Discrete signal processing on graphs: Frequency analysis," *IEEE Trans. Signal Process.*, vol. 62, no. 12, pp. 3042–3054, Jun. 2014.

[17] A. Anis, A. Gadde, and A. Ortega, "Towards a sampling theorem for signals on arbitrary graphs," in *Proc. IEEE Int. Conf. Acoust., Speech Signal Process. (ICASSP)*, May 2014, pp. 3864–3868.

[18] S. Chen, R. Varma, A. Sandryhaila, and J. Kovačević, "Discrete signal processing on graphs: Sampling theory," *IEEE Trans. Signal Process.*, vol. 63, no. 24, pp. 6510–6523, Dec. 2015.

[19] X. Wang, J. Chen, and Y. Gu, "Generalized graph signal sampling and reconstruction," in *Proc. IEEE Global Conf. Signal Inf. Process. (GlobalSIP)*, Dec. 2015, pp. 567–571.

[20] A. Anis, A. Gadde, and A. Ortega, "Efficient sampling set selection for bandlimited graph signals using graph spectral proxies," *IEEE Trans. Signal Process.*, vol. 64, no. 14, pp. 3775–3789, Jul. 2016.

[21] S. Chen, R. Varma, A. Singh, and J. Kovacević, "Signal recovery on graphs: Fundamental limits of sampling strategies," *IEEE Trans. Signal Inf. Process. Netw.*, vol. 2, no. 4, pp. 539–554, Dec. 2016.

[22] F. Wang, Y. Wang, and G. Cheung, "A-optimal sampling and robust reconstruction for graph signals via truncated neumann series," *IEEE Signal Process. Lett.*, vol. 25, no. 5, pp. 680–684, May 2018.

[23] L. F. O. Chamon and A. Ribeiro, "Greedy sampling of graph signals," *IEEE Trans. Signal Process.*, vol. 66, no. 1, pp. 34–47, Jan. 2018.

[24] A. Ortega, P. Frossard, J. Kovačevič, J. M. F. Moura, and P. Vandergheynst, "Graph signal processing: Overview, challenges, and applications," *Proc. IEEE*, vol. 106, no. 5, pp. 808–828, May 2018.

[25] F. Grassi, A. Loukas, N. Perraudin, and B. Ricaud, "A time-vertex signal processing framework: Scalable processing and meaningful representations for time-series on graphs," *IEEE Trans. Signal Process.*, vol. 66, no. 3, pp. 817–829, Feb. 2018.

[26] S. Segarra, A. G. Marques, G. Leus, and A. Ribeiro, "Reconstruction of graph signals through percolation from seeding nodes," *IEEE Trans. Signal Process.*, vol. 64, no. 16, pp. 4363–4378, Aug. 2016.

[27] M. Tsitsvero, S. Barbarossa, and P. Di Lorenzo, "Signals on graphs: Uncertainty principle and sampling," *IEEE Trans. Signal Process.*, vol. 64, no. 18, pp. 4845–4860, Sep. 2016.

[28] P. Di Lorenzo, P. Banelli, S. Barbarossa, and S. Sardellitti, "Distributed adaptive learning of graph signals," *IEEE Trans. Signal Process.*, vol. 65, no. 16, pp. 4193–4208, Aug. 2017.

[29] E. Isufi, P. Banelli, P. Di Lorenzo, and G. Leus, "Observing bandlimited graph processes from subsampled measurements," in *Proc. 52nd Asilomar Conf. Signals, Syst., Comput.*, Oct. 2018, pp. 168–174.

[30] E. Isufi, P. Banelli, P. Di Lorenzo, and G. Leus, "Observing and tracking bandlimited graph processes," 2017, *arXiv:1712.00404*. [Online]. Available: https://arxiv.org/abs/1712.00404

[31] H. Zhang, R. Ayoub, and S. Sundaram, "Sensor selection for Kalman filtering of linear dynamical systems: Complexity, limitations and greedy algorithms," *Automatica*, vol. 78, pp. 202–210, Apr. 2017.

[32] X. Xie, Q. Zhou, D. Hou, and H. Zhang, "Compressed sensing based optimal sensor placement for leak localization in water distribution networks," *J. Hydroinformatics*, vol. 20, no. 6, pp. 1286–1295, Nov. 2018.

[33] N. D. Sidiropoulos and A. Kyrillidis, "Multi-way compressed sensing for sparse low-rank tensors," *IEEE Signal Process. Lett.*, vol. 19, no. 11, pp. 757–760, Nov. 2012.

[34] X. Ding, W. Chen, and I. J. Wassell, "Joint sensing matrix and sparsifying dictionary optimization for tensor compressive sensing," *IEEE Trans. Signal Process.*, vol. 65, no. 14, pp. 3632–3646, Jul. 2017.

[35] A. Sandryhaila and J. M. F. Moura, "Big data analysis with signal processing on graphs: Representation and processing of massive data sets with irregular structure," *IEEE Signal Process. Mag.*, vol. 31, no. 5, pp. 80–90, Sep. 2014.

[36] A. M. Lyapunov, "The general problem of the stability of motion," *Int. J. Control*, vol. 55, no. 3, pp. 531–534, 1992.

[37] G. Moutsinas and W. Guo, "Node-level resilience loss in dynamic complex networks," 2018, *arXiv:1808.05975*. [Online]. Available: https://arxiv.org/abs/1808.05975

[38] A. Pagani, G. Mosquera, A. Alturki, S. Johnson, S. Jarvis, A. Wilson, W. Guo, and L. Varga, "Resilience or robustness: Identifying topological vulnerabilities in rail networks," *Roy. Soc. Open Sci.*, vol. 6, no. 2, Feb. 2019, Art. no. 181301.

[39] A. Yazdani and P. Jeffrey, "Complex network analysis of water distribution systems," *Chaos*, vol. 21, no. 1, Mar. 2011, Art. no. 016111.

ZHUANGKUN WEI was born in Beijing, China, in 1993. He received the bachelor's and master's degrees in electronic engineering from the Beijing University of Posts and Telecommunications (BUPT), Beijing, in 2014 and 2018, respectively. He is currently pursuing the Ph.D. degree with the School of Engineering, The University of Warwick. His research interests include graph signal processing and molecular communication.

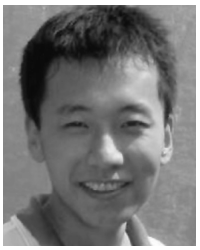

BIN LI received the bachelor's degree in electrical information engineering from the Beijing University of Chemical Technology (BUCT), in 2007, and the Ph.D. degree in communication and information engineering from the Beijing University of Posts and Telecommunications (BUPT), in 2013.

He joined BUPT, in 2013, where he is currently an Associate Professor with the School of Information and Communication Engineering (SCIE). He has published more than 70 journal and conference papers. His current research interests include statistical signal processing for wireless communications, such as molecular communications, millimeter-wave (mm-wave) communications, and cognitive radios (CRs). He received the 2010 and 2011 BUPT Excellent Ph.D. Student Award Foundations, the 2011 ChinaCom Best Paper Award, and the 2015 IEEE WCSP Best Paper Award. He serves as the Co-Chair for the Technical Program Committee of the Signal Processing for Communications Symposium at the 2016 IEEE International Conference on Computing, Networking and Communications (IEEE-ICNC 2016).

WEISI GUO (S'07–M'11–SM'17) received the M.Eng., M.A., and Ph.D. degrees from the University of Cambridge.

He was an Associate Professor with the School of Engineering, University of Warwick. He is currently the Chair Professor of human machine intelligence with the School of Aerospace, Transport, and Manufacturing, Cranfield University. He has published over 130 articles. He was the PI on over 2.3 M of research grants from EPSRC, H2020, the Royal Society, Innovate U.K., and DSTL. His research interests include network science, molecular communications, and complexity theory. His research has won him several international awards (Bell Labs Prize Finalist 2014, IET Innovation 2015, and a Semi-Finalist, in 2016 and 2019), as well as the Turing Fellowship from the Alan Turing Institute.